remote sensing

MDPI

Article

Mapping Urban Functional Zones by Integrating Very High Spatial Resolution Remote Sensing Imagery and Points of Interest: A Case Study of Xiamen, China

Jinchao Song [1,2,*], Tao Lin [1], Xinhu Li [1,*] and Alexander V. Prishchepov [2]

[1] Key Lab of Urban Environment and Health, Institute of Urban Environment, Chinese Academy of Sciences, Xiamen 361021, China; tlin@iue.ac.cn

[2] Department of Geosciences and Natural Resource Management, University of Copenhagen, 1350 Copenhagen, Denmark; alpr@ign.ku.dk

* Correspondence: songjinchao08@163.com (J.S.); xhli@iue.ac.cn (X.L.)

Received: 19 September 2018; Accepted: 1 November 2018; Published: 3 November 2018

Abstract: Fine-scale, accurate intra-urban functional zones (urban land use) are important for applications that rely on exploring urban dynamic and complexity. However, current methods of mapping functional zones in built-up areas with high spatial resolution remote sensing images are incomplete due to a lack of social attributes. To address this issue, this paper explores a novel approach to mapping urban functional zones by integrating points of interest (POIs) with social properties and very high spatial resolution remote sensing imagery with natural attributes, and classifying urban function as residence zones, transportation zones, convenience shops, shopping centers, factory zones, companies, and public service zones. First, non-built and built-up areas were classified using high spatial resolution remote sensing images. Second, the built-up areas were segmented using an object-based approach by utilizing building rooftop characteristics (reflectance and shapes). At the same time, the functional POIs of the segments were identified to determine the functional attributes of the segmented polygon. Third, the functional values—the mean priority of the functions in a road-based parcel—were calculated by functional segments and segmental weight coefficients. This method was demonstrated on Xiamen Island, China with an overall accuracy of 78.47% and with a kappa coefficient of 74.52%. The proposed approach could be easily applied in other parts of the world where social data and high spatial resolution imagery are available and improve accuracy when automatically mapping urban functional zones using remote sensing imagery. It will also potentially provide large-scale land-use information.

Keywords: GF-2 remote sensing imagery; POIs; functional zone; land-use classification

1. Introduction

Urbanization in developing countries has progressed rapidly over the past 20 years [1]. According to the World Urbanization Prospects, issued by the Department of Economic and Social Affairs of the United Nations Secretariat, the global proportion of urban population increased from 30% in the 1950s to more than 54% in 2014. Rapid urbanization has caused a dramatic change in land-use [2,3], population density, and environmental pollution [4]. There has been increasing demand for fine-scale urban functional zone maps, which are the basic units for quantitative analyses in urban transportation, job accessibility, and residential relocation, as well as being used in economic [5] and demography studies over the past few decades [6]. Specifically, the spatial pattern of urban functional zones influences the efficiency of urban life. The relationship between urban functions and human mobility is important for determining the demand for people in different urban functions

and the current availability in an urban space area [7]. The sharp division of functional zones leads to the separation of workplaces and residences, and urban problems such as traffic jams, "sleeping districts", and air pollution [8,9]. However, most functional zone datasets derived from field studies are time-consuming to collect and hard to update at a later point. The availability of multispectral satellite remote imagery and big data, such as information on traffic and the utilization of cellular mobile phone networks, provides great potential in mapping urban functional zones [10]. To combine these data, an efficient approach to mapping the detailed functional zones is required that combines spectral and texture components from multi-spectral remotely sensed imagery and data about the anthropogenic activity (land use).

Remote sensing techniques have been recognized as vital for mapping urban land use changes [11–14] because of their ability to capture the physical characteristics of land-use [15]. In particular, high spatial resolution remote sensing images have resulted in an increase in detailed urban land-use identification [16–19]. Furthermore, object-based image analysis methods are suitable for the classification of medium and high spatial resolution imagery and provide a valid alternative to pixel-based methods of analyzing and categorizing remote sensing data [20]. Generally, two kinds of approaches to land-use classification have been applied in the literature: (1) Use of land-use indicators. Land use indicators mainly include the proportion of land-cover, but also the density of land cover features. However, land-use indicators fail to effectively characterize land use in complex urban areas such as shopping centers, residential buildings, and business office buildings because they mainly consider spectral characteristics, coverage ratios, and the densities of land-use features. In addition, shadows and dark roofs may have similar spectral, textual, and geometrical characteristics, resulting in a high misclassification rate among different urban land uses [17]. (2) The other is based on spatial arrangements. The spatial arrangement (also called spatial layout) of land-use features characterized by quantifying the distribution of building types can effectively improve urban land-use extraction performance [16,21–24] and spatial arrangement information of local features is important for the application of scene classification (e.g., a railway station or an airport) [25–27]. However, training samples based on the spatial arrangement of buildings (segments or objects) are restricted by the different types of roofs or architecture styles across cities [17]. Thus, such approaches often provide limited model training information for urban functional zone on a broader scale. Mapping urban land use with remotely sensed imagery is more difficult in built-up areas because most remotely-sensed imagery merely records the natural characteristics of land cover, which can be associated with electromagnetic reflectance, and further assessed with texture measures or grouped into broad classes, such as "forest" or "built up". This poses a deficiency in information about human and social activities. Therefore, remote sensing imagery alone cannot identify inner-building attributes, so it is necessary to explore an effective way to combine the useful characteristics of remote sensing images and social sensing data.

Big data have advantages in urban studies due to their immediacy, volume, and social attributes. The big social data with spatial attributes (e.g., with geographic coordinates) can be collected from all kinds of handset devices, such as GPS, mobile phones, include static and dynamic datasets. Static data mainly include points of interest (POIs) which could provide detailed land use information based on human activity acquired from online maps and some social media (e.g., Facebook, Twitter). From the point view of the application, road networks from open street maps and POI data are employed to infer parcel characteristics [28], construct 3D models [29], and classify urban commercial districts at the parcel scale [30]. Dynamic datasets are used to build models to cluster segmented regions into functional zones and identify the intensity of the functional zone, for instance, mobile phone data, social media on internet, and transportation information [7,31]. Mobile phone record data have been used to analyze urban spatial structure [15] and patterns of population mobility [7,32–35], as well as to analyze job–housing relationships [36]. Only a few studies have classified urban land-use by combining remote sensing imagery and social media data [37–40]. Some approaches [6,7,15,22] utilized the numbers of POIs or quantified location-based service (LBS) data instead of using polygon

of building roof to map functional boundaries. However, as the POIs density varies in different zones, using point quantification and excluding building boundaries could reduce the accuracy of the results. Study on mapping urban land use using Landsat images and open social data also indicated that the low spatial resolution imagery could not map the detailed information, especially in irregular spatial arrangement areas such as public areas and shopping centers [39,41]. High spatial resolution imagery could fill the gap and provide detailed texture of the building roof [42].

Our overarching goal was to map functional zones using high-resolution remote sensing imagery and POIs. To do so, our first objective was to map the building roof-based segments using very high-resolution remotely-sensed imagery and append the attributes of POIs to the segments. The second step was to map the functional zones based on a unit of parcels which were generated with road network and functional segments. Then, we analyzed the spatial pattern of functional zones by using an example from Xiamen, China.

2. Methods

The workflow (Figure 1) of mapping functional zones includes five parts: (1) Urban land cover classification; (2) segmentation of imagery to obtain polygons corresponding to the roof of building; (3) appending the function of POIs to the segmentation to obtain a functional segmentation; (4) appending functional segmentation to parcels to obtain the functional parcels; (5) assessing the accuracy using validation points. To improve the accuracy, we experimented with different values of the parameters for image segmentation, the weight coefficients of the functional POIs, and the functional segmentation.

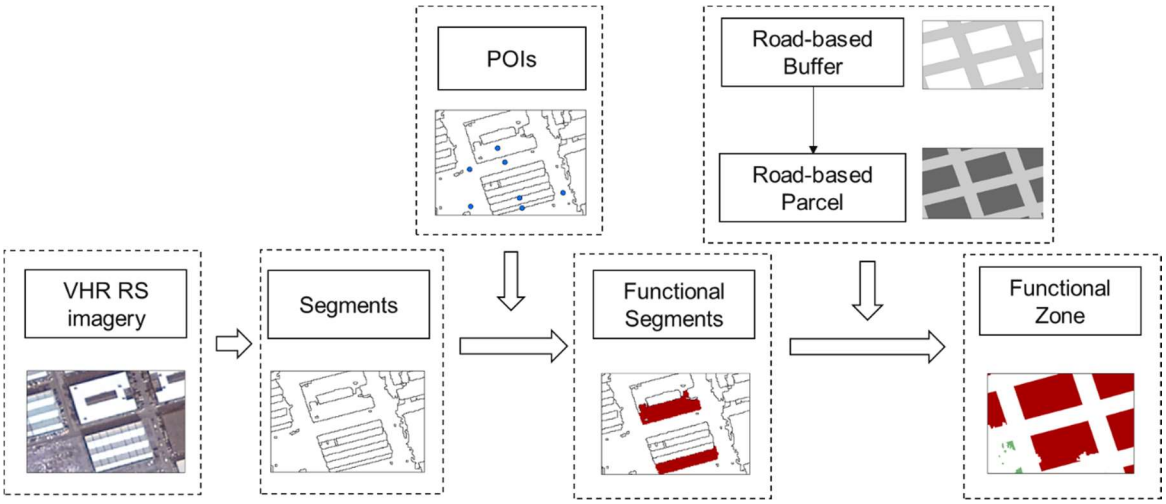

Figure 1. The workflow of mapping functional zones.

2.1. Urban Land Cover Classification and the Generation of Functional Parcels

To improve the accuracy of extracting functional zones in built-up areas, we first used high spatial resolution satellite imagery to produce a binary built-up/non-built-up land cover map using an example-based feature extraction in ENVI 5.1 [43]. The non-built area covered the water, grass, and forest and built-up area. All roofs with different reflectance were considered built-up areas, such as factories with blue roofs and residential buildings with red or grey roofs, in R, G, B natural-color combination. We used an object-based approach in which one object is a group of pixels with similar spectral, spatial, or texture attributes. To find optimal parameters for image segmentation for classifying built-up area we utilized Edge method in ENVI5.1 software and experimented with a series of image segmentation settings, namely edge and full lambda schedule. As most of the POIs and functional zones cluster in built-up areas, we masked out non-built area. The road network was acquired from Baidu map. Then based on the width of different road types, we generated the parcels using the buffer

tool. The buffer size depends on road grade design in different cities. The segmentation and parcels in a built-up area were used as the input dataset for functional calculations.

2.2. Image Segmentation on Buildings

To fine-tune segmentation for building rooftop in built-up area, we refined the analysis with new parameters of segmentation. Within the built-up area, primarily buildings and associated land use determine the urban functional zones. The goal of multi-resolution segmentation is for each pixel of a building to belong to a certain segment [44]. For the best segmentation results and effective feature delineation, we set an appropriate scale level and merge level for detecting the edges of features, based on experimenting with parameter selection in ENVI 5.1. The optimum scale level effectively delineates the boundaries of the features without over-segmenting the features but merging combined adjacent segments with similar spectral attributes. We used a full lambda schedule algorithm to merge the small segments found within larger and textured areas. Where a building roof might consist of several segments, we chose a faster lambda and increased the merge level to combine similar objects into one segment. The greater the merge level parameter, the more heterogeneity is allowed within each object and the larger the average size of the objects [45]. The process stops when there are no more possible merges, given the defined segment size [46].

2.3. The Weights of POIs and Segmentation

To balance the discrepancy between the main and affiliated functions of parcels, we identified their functional attribute from their POIs, segmentation, and weights. For instance, one segment polygon may cover one or two POIs, or different kinds of functional segmentation may exist in one parcel. An airport may contain multiple POIs, but only few POIs may have an attribute "airport". The weights of the POIs and segmentation were calculated with the Delphi consensus technique, which has been applied in natural resources and city management research to investigate a variety of local, regional, and global issues [47–50]. The Delphi technique involves a survey using questionnaires with feedback from the panel of experts to develop indicators in a study. We applied this technique in two steps: (1) an expert panel with a sufficient knowledge and experience in urban studies and planning was established and asked to comment via the questionnaire; (2) 15 questionnaires were sent to participants to determine the importance of each indicator. After collecting the scores from the first round, the experts were presented with the feedback results for each indicator and gave new rates. The results of the second round represented the alternative ranking.

Table 1. The weights of points of interest (POIs): first and second round. Smaller numbers indicate a higher priority with a range from 1 to 9.

Indicators	Previous Judgment	First Round	Second Round	Result of Priority
Transportation Zone	2	2	1	1
Shopping Center	1	1	2	2
Public Service Zone 1	3	4	3	3
Residence	5	3	4	4
Factory	6	5	6	5
Company	4	6	5	6
Public Service Zone 2	7	7	7	7
Public Service Zone 3	8	8	8	8
Convenience Shop	9	9	9	9

2.4. Appending the Function of POIs to Segmentation

The functions of the segmentation were defined by the weights and numbers of the POIs, where smaller numbers represented the higher priority (Table 1). For instance, if airport and convenience shop points are present in a segment simultaneously, the functional attribute will be defined as a transportation zone (Table 1, row 1). Following these rules, we joined the attributes from POIs

to segments based on the spatial relationship to finally obtain the functional segments (segments with function).

2.5. Appending Functional Segmentation to Parcels

Based on the weights of the segmenting function, the functional segmentations were appended to the road network-based parcels based on the spatial relationship according to the following rules:

A. Firstly, the transportation zone and shopping center should be the primary function. If there is a transportation zone (such as an airport or railway station) and a shopping center in the same parcel, the main function of this parcels is transportation and the shopping center is secondary.
B. If there is no transportation or shopping center point in a parcel, the method of determining the function would obey the following rule:

$$R = Maximum\ (Ai \times Wi\ ) \quad (1)$$

where A_i represents the number of functional segmentations for type i, W_i represents the functional segmentation weight (Table 2), and R refers to the main function in a parcel.

Table 2. The weights of the segmenting function with a range from 1 to 9: first and second round.

Indicators	Previous Judgment	First Round	Second Round	Result of Score
Transportation Zone	1	1	1	1
Shopping Center	1	1	1	1
Public Service Zone 1	0.3	0.62	0.4	0.55
Residence	0.2	0.2	0.43	0.34
Factory	0.1	0.05	0.1	0.06
Company	0.1	0.04	0.02	0.024
Public Service Zone 2	0.15	0.01	0.03	0.015
Public Service Zone 3	0.1	0.02	0.01	0.01
Convenience Shop	0.05	0.06	0.01	0.001

2.6. Accuracy Assessment

To assess accuracy for thematic classes, non-built (grass, forest and water body) and built-up area, including transportation, factory, residence and business, public service 1, public service 2, and public service 3, we constructed confusion matrix and calculated overall (OA), user's (UA) and producer's accuracies (PA). Confidence interval (error tolerance) is computed according to [51] with the confidence level of 90%:

$$Interval = 1.64 * \sqrt{A * (1 - accuracy)/n} \quad (2)$$

where n is the cardinality of the reference data collected by field work, A is classification accuracy of different class.

3. Case Study

3.1. Study Area

Xiamen is an island, which became one of the four special economic zones in China established in 1980 with special investment and trade regulations. Xiamen became a sub-provincial city in southeastern China whose urban core area grew up from the port of Xiamen on southern Xiamen Island and experienced a fast urbanization process during the past 30 years [41]. According to the 2010 Census, Xiamen has a population of 3.5 million inhabitants, which increased 1.8 times from the last census in 2000. The annual average population growth rate was of 5.57% for the period 2000–2010. Due to land scarcity, reclamation offered space for urban built areas in the southwest of the island along the lakeside, while public service facilities and railway stations were built around existing residential zones. We chose Xiamen Island as our study area (approximately 136.3 km^2) because we

could extract various POIs representing different functional zones (Figure 2). Urban communities and new residential parcels appeared along the southwest coast. Nowadays, tourism is the third largest industry and therefore some artistic villages with compact houses remain clustered in the city center for residency and shopping purposes. As a sub-provincial city, new urban and industrial areas were developed in the northeastern part of the island [41].

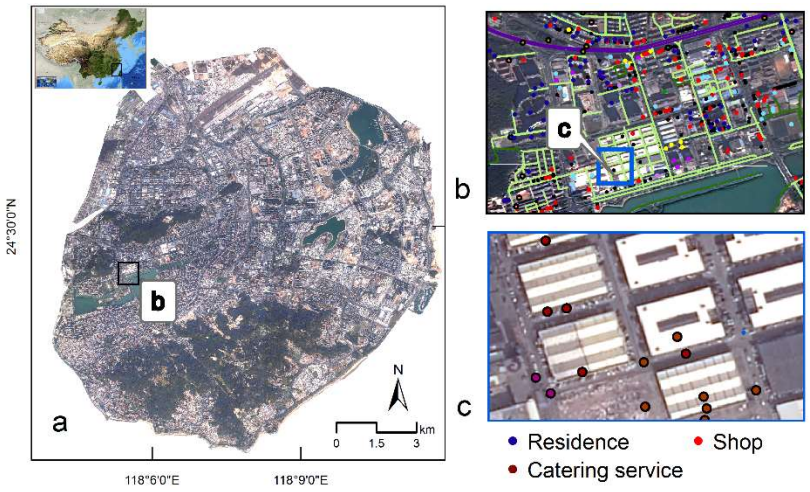

Figure 2. (**a**) High-resolution images from GaoFen-2 (GF-2) covering Xiamen Island; (**b**) a sample area showing detailed information about points of interests (POIs) and roads; (**c**) a sample area showing detailed information about POIs overlaid with buildings.

3.2. Data Source and Preprocessing

3.2.1. GaoFen-2 Remote Sensing Imagery

The high spatial resolution remote sensing imagery used in this research was acquired from the GaoFen-2 (GF2) satellite, which was launched by the China National Space Administration on 19 August 2014. Its spatial resolution of the panchromatic band is 1 m and for its multi-spectral bands (B 0.45–0.52 μm, G 0.52–0.59 μm, R 0.63–0.69 μm, and NIR 0.770–0.89 μm) is 4 m. The width of imagery is 45 km and coverage period is 69 days. We preprocessed two remote sensing images, which were acquired on 16 April 2015 and 6 February 2015, covering 158 km^2. The reason for using imagery from this period was because of fewer clouds during winter and spring season compared to other seasons in Xiamen. Preprocessing of the GF-2 imagery, including radiation calibration, atmospheric correction, orthorectification, and image enhancement, imagery mosaic was performed using ENVI 5.1 software. The multispectral bands were fused with panchromatic bands using the Gram-Schmidt pan-sharpening method with retained multi-spectral characteristics with a spatial resolution of 1 m [42] (Figure 1a).

3.2.2. POIs and Functional Classification

The POIs were obtained through application programming interface operated by Baidu^{TM} which is a company providing service of search engine and maps. The Location Search Service (aka Place API) is a type of Web API interface service; The service provides location-based (POI) retrieval capabilities for a variety of scenarios, including city retrieval, circular area retrieval, and rectangular area retrieval. Developers can obtain location (POI) basis or detailed geographic information through the interface using request parameter, such as the name of the site, detailed classification of the function, and geographic coordinates. The service also provides industry classification of POIs, including primary industry classification and secondary industry classification. In this research, 37,356 points were retrieved from Location Search Service in April 2015 and used to classify the urban functional zones as residences, transportation zones, convenience shops, shopping centers, factories, companies, public

service 1, public service 2, and public service 3. The results of the functional zone classification are shown in Table A1. We set the 8 m to create buffer for expressway and the 4 m to create buffer for branch road. To get the road-based parcel, we use the road buffer to erase the research area polygon.

3.2.3. Data for Training and Validation

The accuracy was assessed using 2134 stratified random sampling points recorded by a non-differential GPS with geotagged photos during field visits, including 1021 samples for the non-built area and 1113 samples for built-up area classification, and 1035 random samples for validating functional zone classification. Field visits were made to each validation point to assign the classes.

4. Results

4.1. Land Cover

Based on visual inspection we chose the edge parameter as 42, the full lambda schedule as 91 and kernel size as 3 resulting in 373,437 objects in the total research area. One thousand and twenty-one samples (303 samples for training and 728 for validation) for non- built- up area and 1113 samples (412 for training and 701 for validation) for built-up area were used to train the samples and assess the accuracy of the land cover classification, respectively. The result is shown in Figure 3. The overall accuracy for classifying built-up and non-built-up areas was 92.2% and the kappa coefficient was 89%. Figure 3d,e show the road buffer and road-based parcel.

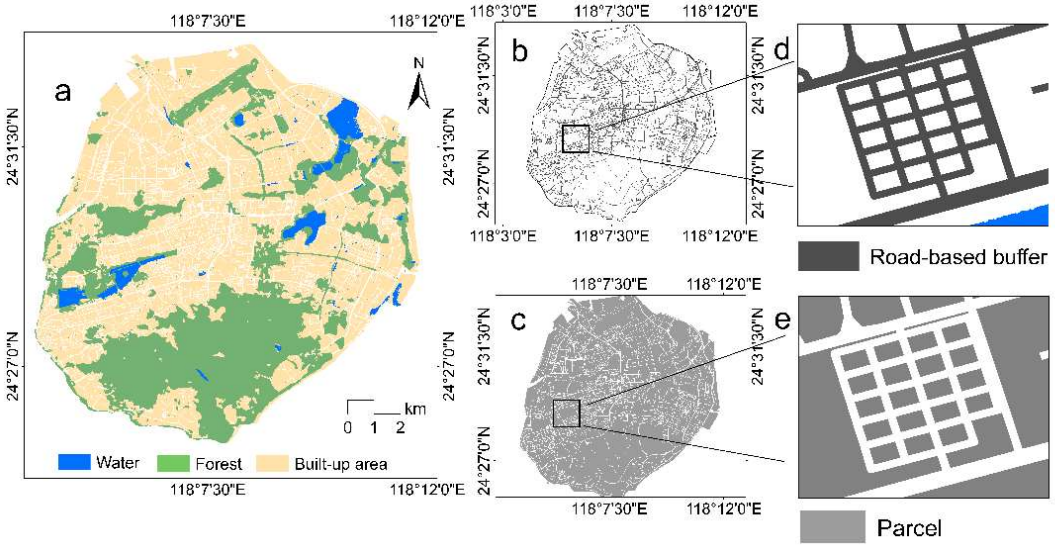

Figure 3. (**a**). The result of the land cover classification (**b**). Road network-based buffer (**c**). Road-based parcel (**d**) Detailed information on road buffer (**e**). Detailed information on road-based parcel.

4.2. Segmentation, Functional Segmentation and Urban Functional Zones

Figure 4 shows the experiment results of segmentation at three levels, based on the different density of buildings after the repeated experiments. When the edge in the algorithm was 40 and the full lambda schedule was 80, this yielded several segments in the same building roof polygon. In this case, the POIs were merely identified by a small segment of one building roof. Likewise, when the edge in the algorithm was 41 and the full lambda schedule was 98, many segments of building roofs were missed when it was conducted on the imagery which was dominated by the dense and high building. In such a situation, the POIs cannot totally be added to the relative spatial polygon of the building. Therefore, according to the requirement of the segment size and the series of experiment results, the parameters were set to produce the highest accuracy, that is, the edge in the algorithm, the full lambda schedule, and the texture kernel size was set as 42, 92.8, and 3, respectively. Figure 5

shows the results of functional segmentation, based on joined attributes from POIs to segments based on the spatial relationship. The weights from the functional segmentation and rules for appending the functional segmentation to the parcels were applied to classify the functional parcels (functional zones) (Figure 6).

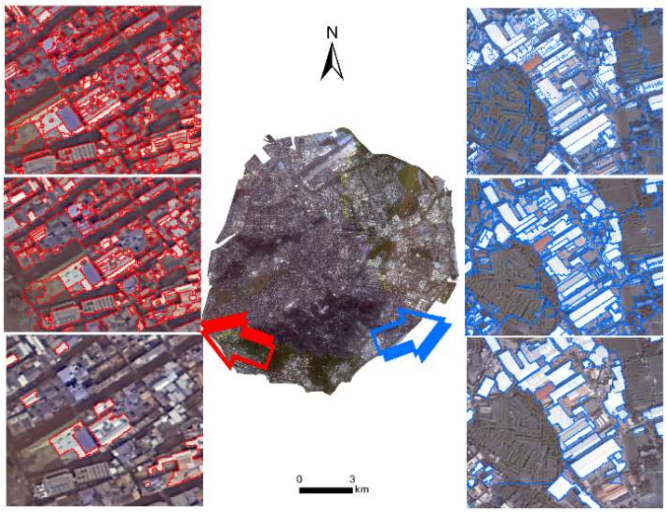

Figure 4. The segmentation at three levels in two areas (red represents a dense and high building area, blue represents a dense area but with low buildings), the parameters algorithm 'edge' and 'full lambda schedule' from top to bottom are 40 and 80, 42 and 92.8, and 41 and 98.

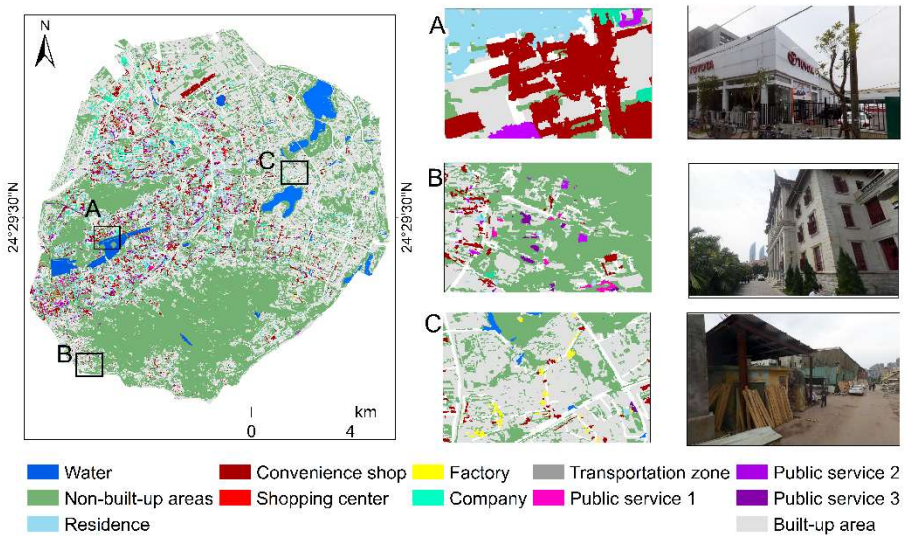

Figure 5. The functional segment identified by the POI and weight coefficients and detailed information; **A.** The convenience shop zone: the car sales area. **B**. The public service zone: campus of university **C**. Factory.

4.3. Accuracy Assessment

A confusion matrix was calculated based on the field investigating the dataset (Table 3). This result showed that the urban functional zone extraction had an overall accuracy of 78.5% and a kappa coefficient of 74.5%. The highest producer's accuracy (93%) was for the factory zone and the lowest (50%) for the convenience shops. The lowest user's accuracy (63%) was for the residence zone. The accuracy for most other functional zones was more than 80%. The confidence interval (error tolerance) of each class accuracy are as listed: residential (3.4%), convenience shops (5.7%),

shopping center (9.2%), factory (5.9%), company (6.1%), and transportation (12%), PS1 (6.9%), PS2 (5.7%), and PS3 (5.2%), the error tolerance of overall accuracy is 6%.

Table 3. The confusion matrix of the urban functional zone extraction. PS1, PS2, and PS3 indicate public service 1, public service 2, and public service 3, respectively. PA and UA refer to the producer and user accuracies of the confusion matrix, respectively.

Classified Data	Reference Data									
	Residence	Convenience Shops	Shopping Center	Factory	Company	Transportation	PS1	PS2	PS3	UA
Residence	218	87	1	14	9	0	0	2	16	63%
Convenience shops	5	100	0	0	2	0	1	4	25	73%
Shopping center	12	0	36	0	3	0	0	0	0	71%
Factory	2	0	0	180	0	0	0	6	7	92%
Company	7	0	0	0	80	1	2	7	3	80%
Transportation	0	0	2	0	0	18	0	0	0	90%
PS1	0	0	0	0	1	2	45	0	4	87%
PS2	2	4	2	0	1	0	2	97	0	89%
PS3	5	9	1	0	0	0	0	2	141	89%
Total	255	200	40	50	100	20	50	120	200	
PA	87%	50%	85%	93%	83%	86%	90%	82%	72%	

Overall accuracy ± error tolerance = 78.47% ± 6%, kappa coefficient = 74.52%.

4.4. The Pattern of Functional Zones

Our results showed the built-up area covered 76.14 km^2. Built up areas covered the largest percentage of the research area (96.3 km^2) and shopping centers were uniformly distributed around the residential zone (27.5 km^2) (Figure 6, Table 4). We observed clusters of convenience shops and wholesale markets for various products, which covered 5.2 km^2 (6.8%). Public service facilities (12.1 km^2) and shopping centers (9.74 km^2) were clustered in the southwest of the island and the industrial, and company zones were clustered in the northern island. Company zone (15.6 km^2) and factory zone (4.1 km^2) are located at the northern part of Xiamen Island, and the transportation zone, including the airport and railway station, covers 1.9 km^2.

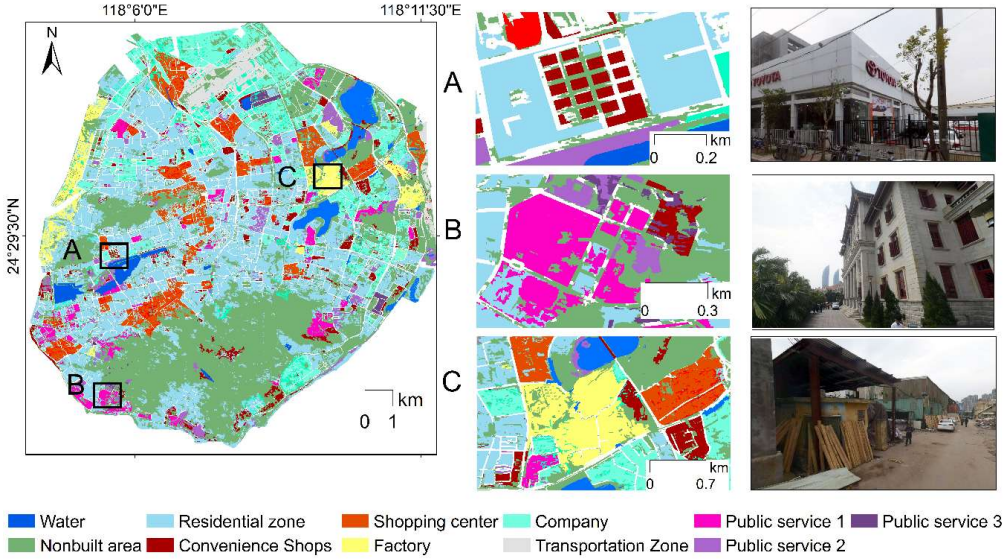

Figure 6. The result of the functional zone classification and detailed information; **A**. The convenience shop zone: the car sales area. **B**. The public service zone: the campus of university **C**. Factory.

Table 4. Area and proportion of different functional zones.

Functional Zone	Area (km^2)	Proportion
Residence	27.5	36.1%
Convenience shops	5.2	6.8%
Shopping center	9.74	12.8%
Factory	4.1	5.3%
Company	15.6	20.5%
Transportation	1.9	2.5%
Public Service	12.1	15.9%

5. Discussion

5.1. Analysis of the Accuracy Measures

Our analysis showed that urban functional zones could be extracted from high-resolution remote sensing imagery with the aid of POIs with reasonable accuracy of 78.47%. However, such high classification accuracies with fine classifications required several factors: the segment parameter, the weight coefficient, the road network density, and data fusion of POIs and high-resolution remote sensing imagery. The approach we proposed can be applied to many countries, where POIs are available. Our results also show that the high-resolution multi-spectral imagery, like GF-2 with 1-meter spatial resolution, allow the accurate segmentation of different building roofs and provide accurate building rooftop polygon for combining with POIs.

Analysis with the object-based classification approach revealed that segmentations create objects representing land use types that may be spectrally variable at the pixel level and this was influenced by three parameters: scale, reflectance (color or tone) and shape. The color parameter balances the homogeneity of a building's roof color with the homogeneity of its shape. The shape parameter balances the smoothness of a segment's border and compactness. Therefore, object-based classification approximates the real world features better than pixels [52]. If the segmentation is divided coarsely, it may undersegment the image with noticeable mixtures of building roofs and covers; the redundant surface features and the segmentation result would be sketchy and low in accuracy. If the segmentation is divided in a detailed manner, oversegmenting the image with many adjacent objects of building roofs and many segment polygons would miss the POIs. In addition to the segment parameters, accurate weight parameters for the identification of functional segments and functional parcels were important. When the weights of the functional segmentation were adjusted, the accuracy of the assignment of function to zones varied markedly because the main function with a few POIs could be replaced by an auxiliary function with a high density of POIs—if no difference or a lower difference existed in the weight coefficients. The reason for using the segment to extract the segmental functional zone instead of using parcels directly is that some convenience shops along the road serving the main function of this parcel are auxiliary facilities, such as a barbershop or the restaurants near residence zones or railway stations. Therefore, it is necessary to balance the numbers of the main and auxiliary functional POIs. However, it is difficult to define the weights of different kinds of functional POIs directly. For example, 30 POIs identifying a convenience shop were around the railway station, while only five points of the convenience shops were around the residence zone. Therefore, it is effective to use functional segmentation as an intermediate product to map functional parcels. Based on the combination of segments and POIs, the UA of the industrial zone (92%) and public service zone (87%) were improved compared to conventional methods (58%, 82%) [39]. However, UA for the residential zone was still low, since the residential zone class could overlap with public service 3 (kindergarten) and convenience shops thematic classes.

We also found that the road density influenced the accuracy of functional zone extraction. The accuracy is lower in sparse road areas than in areas with a density of roads because in the former case the parcel will cover more types of POIs and functions. Therefore, the accuracy would be

higher if applied in the city center, which has a high density of POIs. In a condition where no POIs are related with a residential use and there are some small stores as auxiliary functions located at the first floor of a building, the building will be incorrectly classified as a convenience shop. Some residential buildings are dormitories for workers to work conveniently in factory zones. Thus, the auxiliary zones could be confounded and increase the error tolerance of residential area (3.4%). Even though the building roof of a railway station could be easily extracted using remote sensing images, the transportation zone with higher confidence interval of 12% is still confused with the shopping center zone because some shopping malls are present around the Xiamen railway station and, furthermore, the railway station was being rebuilt during the research period, with bare soil replacing the roof of the station building in the remote sensing images (Figure 5c). The shopping center class has a high producer accuracy (85%), but its error tolerance is 9.2%. Here are the possible reasons. City planning and development usually take a unit of road-based parcel. The government focuses on improving the intensive land use level and urban complex. So, the residential area and company may exist within a shopping center in one building. These fusions challenge the functional zone classification accuracy in a built-up area. Therefore, functional arrangement influences accuracy when mapping functional zones, and it is necessary to update the weights of functional segmentation when applying the method to other cities, especially cities with different architecture morphology.

5.2. Other Methodological and Applied Considerations

Considerable effort has been made in recent years to improve the accuracy of mapping land use in an urban area [52,53]. Remote sensing imagery and big social data have usually been applied separately in urban studies. Land-use classification for remotely sensed images was based on the spectral information of pixels and objects. Most experiments concentrate on several classes, including buildings, streets, open areas, residential lawns, and shadows [21]. The application of big social data to map local functional zones was lacking information on spatial boundaries, losing insight into the functional proportions of spatial heterogeneity [28,36]. In this research, we took full advantage of very high spatial resolution remotely sensed imagery to segment the building rooftop and appended points with functions into the polygons of the building roof and, furthermore, bridged the gap between dominant points and non-major points to balance the proportion of the function for improving the accuracy of the application of remote sensing in city areas. A high precision map of a functional zone provides basic data for applied research at a large scale, for instance, urban land use transition, evaluation of urban land intensive use and estimating population density and space distribution of public service facilities, etc. Hence, the approach that used physical features of satellite imagery and POIs produced a more detailed parcel-based functional zones map than the approach that used a single data source and provided the foundation for meticulous city management.

We acknowledge that the accuracy can be improved further. Some office buildings and parcels including markets, companies, and residences were difficult to identify because of their similar shape and building material. Buildings along roads with convenience shops on the ground floor could be bungalows or high-rise buildings. However, we suggest that the building height can be utilized, for instance from LIDAR, high-resolution imagery stereo pairs and other sources. High spatial resolution imagery is still poor in spatial resolving power and often shows weak reflectance around building boundaries. The LIDAR can reliably attribute accurate 3D information to the building boundaries extracted by optical imagery and isolate building regions by subtracting terrain surface [54]. We also noticed that the numbers of POIs and spatial and spectral resolutions of remote sensing images varied in different research areas, especially in the city center and suburb areas. Additionally, the road network is sparser in the suburbs than in the city center. We suggest that the research areas can be classified according to the data volume of the POIs and the density of the road network in order to improve accuracy. With the development of the internet and location-based services, this method could incorporate more kinds of data and, thus, the accuracy of the method would be improved as the number of POIs grows. As for the determination of weights and application in other research areas,

machine learning methods could be applied to train the weights of POIs and functional segmentations instead of using Delphi. Machine learning methods have the potential to improve the accuracy of training samples and classification.

6. Conclusions

We developed an approach to mapping urban functional zones by integrating physical features of high spatial resolution remotely sensed imagery and anthropogenic activity of POIs. To improve the accuracy and mine the detailed social attributes of the buildings, we applied image segmentation to locate the boundaries of building roofs. We then appended functional segmentation to parcels, based on the road networks. The results showed that the fusion of POIs and remotely sensed imagery could refine the classification and improve accuracy in some areas which were difficult to classify with the previous approach. The overall accuracy of the functional zones with 10 classes reached 78.47%. Therefore, we concluded that the proposed method provided an alternative means for mapping urban functional zones using high-resolution images and POIs and could be potentially applied elsewhere.

Author Contributions: Conceptualization, T.L. and J.S.; methodology, software, validation, formal analysis, investigation, J.S.; resources, data curation, X.L. and T.L.; writing—original draft preparation, J.S. and A.V.P.; writing—review and editing, J.S. and A.V.P.; visualization, J.S.; supervision, A.V.P.; project administration and funding acquisition, T.L.

Funding: We would like to acknowledge the financial support of China Scholarship Council foundation, National Science Foundation of China (No. 41671444, No. 41371540), and China High-Resolution Earth Observation System.

Conflicts of Interest: The authors declare no conflict of interest.

Code Availability: The code used for mapping functional zone in this study has been deposited in GitHub: https://github.com/soho1990/Jinchao-Song/tree/master/Functional%20zone.

Appendix A

Table A1. The classification of points of interests (POI).

Function	POI
Residential zone	Commercial residence Residence community
Convenience shop zone	Restaurant Insurance company Shopping service Animal medical center Life service Car sales company Car maintenance company Car service Motorcycle service Financial insurance company Bank Security company Sport service hotel
Shopping center factory Company	Shopping mall/market factory Company in office building

Table A1. *Cont.*

Function	POI	
Public Service Zone	Public service 1	Municipal government University and college Top three hospital
	Public service 2	Middle school Judicial organ Medical care service Second-class hospital Social organization and government agency Scenic zone
	Public service 3	Kindergarten Public learning service
Transportation zone	Airport Railway station	
Non-built-up area	Agricultural land Water Mountain or forest	

References

1. Cohen, B. Urbanization in developing countries: Current trends, future projections, and key challenges for sustainability. *Technol. Soc.* **2006**, *28*, 63–80. [CrossRef]
2. Mallach, A.; Haase, A.; Hattori, K. The shrinking city in comparative perspective: Contrasting dynamics and responses to urban shrinkage. *Cities* **2016**, *69*, 102–108. [CrossRef]
3. Audirac, I. Shrinking cities: An unfit term for American urban policy? *Cities* **2017**, *75*, 12–19. [CrossRef]
4. He, C.; Gao, B.; Huang, Q.; Ma, Q.; Dou, Y. Environmental degradation in the urban areas of China: Evidence from multi-source remote sensing data. *Remote Sens. Environ.* **2017**, *193*, 65–75. [CrossRef]
5. Shin, H.B. Residential redevelopment and the entrepreneurial local state: The implications of Beijing's shifting emphasis on urban redevelopment policies. *Urban Stud.* **2009**, *46*, 2815–2839. [CrossRef]
6. Jiang, S.; Alves, A.; Rodrigues, F.; Ferreira, J.; Pereira, F.C. Mining point-of-interest data from social networks for urban land-use classification and disaggregation. *Comput. Environ. Urban Syst.* **2015**, *53*, 36–46. [CrossRef]
7. Li, M.; Shen, Z.; Hao, X. Revealing the relationship between spatio-temporal distribution of population and urban function with social media data. *GeoJournal* **2016**, *81*, 919–935. [CrossRef]
8. Huang, W.; Fan, H.; Qiu, Y.; Cheng, Z.; Xu, P.; Qian, Y. Causation mechanism analysis for haze pollution related to vehicle emission in Guangzhou, China by employing the fault tree approach. *Chemosphere* **2016**, *151*, 9–16. [CrossRef] [PubMed]
9. Tonne, C.; Halonen, J.I.; Beevers, S.D.; Dajnak, D.; Gulliver, J.; Kelly, F.J.; Wilkinson, P.; Anderson, H.R. Long-term traffic air and noise pollution in relation to mortality and hospital readmission among myocardial infarction survivors. *Int. J. Hyg. Environ. Health* **2016**, *219*, 72–78. [CrossRef] [PubMed]
10. Banzhaf, E.; Hofer, R. Monitoring urban structure types as spatial indicators with CIR Aerial Photographs for a more effective urban environmental management. *IEEE J. Sel. Top. Appl. Earth Obs. Remote Sens.* **2008**, *1*, 129–138. [CrossRef]
11. Coulter, L.L.; Stow, D.A.; Tsai, Y.; Ibanez, N.; Shih, H.; Kerr, A.; Benza, M.; Weeks, J.R.; Mensah, F. Classification and assessment of land cover and land-use change in southern Ghana using dense stacks of Landsat 7 ETM+ imagery. *Remote Sens. Environ.* **2016**, *184*, 396–409. [CrossRef]
12. Gómez, C.; White, J.C.; Wulder, M.A. Optical remotely sensed time series data for land cover classification: A review. *ISPRS J. Photogramm. Remote Sens.* **2016**, *116*, 55–72. [CrossRef]
13. Pagliarella, M.C.; Sallustio, L.; Capobianco, G.; Conte, E.; Corona, P.; Fattorini, L.; Marchetti, M. From one-to two-phase sampling to reduce costs of remote sensing-based estimation of land-cover and land-use proportions and their changes. *Remote Sens. Environ.* **2016**, *184*, 410–417. [CrossRef]
14. Fu, P.; Weng, Q. A time series analysis of urbanization induced land-use and land cover change and its impact on land surface temperature with Landsat imagery. *Remote Sens. Environ.* **2016**, *175*, 205–214. [CrossRef]

15. Pei, T.; Sobolevsky, S.; Ratti, C.; Shaw, S.-L.; Li, T.; Zhou, C. A new insight into land-use classification based on aggregated mobile phone data. *Int. J. Geogr. Inf. Sci.* **2014**, *28*, 1988–2007. [CrossRef]
16. Comber, A.J.; Brunsdon, C.F.; Farmer, C.J.Q. Community detection in spatial networks: inferring land-use from a planar graph of land cover objects. *Int. J. Appl. Earth Obs. Geoinf.* **2012**, *18*, 274–282. [CrossRef]
17. Li, M.; Stein, A.; Bijker, W.; Zhan, Q. Urban land-use extraction from Very High Resolution remote sensing imagery using a Bayesian network. *ISPRS J. Photogramm. Remote Sens.* **2016**, *122*, 192–205. [CrossRef]
18. Pacifici, F.; Chini, M.; Emery, W.J. A neural network approach using multi-scale textural metrics from very high-resolution panchromatic imagery for urban land-use classification. *Remote Sens. Environ.* **2009**, *113*, 1276–1292. [CrossRef]
19. Voltersen, M.; Berger, C.; Hese, S.; Schmullius, C. Object-based land cover mapping and comprehensive feature calculation for an automated derivation of urban structure types at block level. *Remote Sens. Environ.* **2014**, *154*, 192–201. [CrossRef]
20. Benz, U.C.; Hofmann, P.; Willhauck, G.; Lingenfelder, I.; Heynen, M. Multi-resolution, object-oriented fuzzy analysis of remote sensing data for GIS-ready information. *ISPRS J. Photogramm. Remote Sens.* **2004**, *58*, 239–258. [CrossRef]
21. Benediktsson, J.A.; Pesaresi, M.; Arnason, K. Classification and feature extraction for remote sensing images from urban areas based on morphological transformations. *IEEE Trans. Geosci. Remote Sens.* **2003**, *41*, 1940–1949. [CrossRef]
22. Zhi, Y.; Li, H.; Wang, D.; Deng, M.; Wang, S.; Gao, J.; Duan, Z.; Liu, Y. Latent spatio-temporal activity structures: a new approach to inferring intra-urban functional regions via social media check-in data. *Geo-Spat. Inf. Sci.* **2016**, *19*, 94–105. [CrossRef]
23. Zhan, Q.; Molenaar, M.; Tempfli, K. Hierarchical image object-based structural analysis toward urban land-use classification using high-resolution imagery and airborne LIDAR data. In Proceedings of the 3rd International Conference on Remote Sensing of Urban Areas, Istanbul, Turkey, 11–13 June 2002; pp. 11–13.
24. van der Kwast, J.; van de Voorde, T.; Canters, F.; Uljee, I.; van Looy, S.; Engelen, G. Inferring urban land-use using the optimised spatial reclassification kernel. *Environ. Model. Softw.* **2011**, *26*, 1279–1288. [CrossRef]
25. Cheriyadat, A.M. Unsupervised Feature Learning for Aerial Scene Classification. *IEEE Trans. Geosci. Remote Sens.* **2014**, *52*, 439–451. [CrossRef]
26. Chen, S.; Tian, Y. Pyramid of spatial relatons for scene-level land-use classification. *IEEE Trans. Geosci. Remote Sens.* **2015**, *53*, 1947–1957. [CrossRef]
27. Zhao, B.; Zhong, Y.; Zhang, L. A spectral-structural bag-of-features scene classifier for very high spatial resolution remote sensing imagery. *ISPRS J. Photogramm. Remote Sens.* **2016**, *116*, 73–85. [CrossRef]
28. Liu, X.; Long, Y. Automated identification and characterization of parcels with OpenStreetMap and points of interest. *Environ. Plan. B Plan. Des.* **2016**, *43*, 341–360. [CrossRef]
29. Over, M.; Schilling, A.; Neubauer, S.; Zipf, A. Generating web-based 3D City Models from OpenStreetMap: the current situation in Germany. *Comput. Environ. Urban Syst.* **2010**, *34*, 496–507. [CrossRef]
30. Fang, W.; Xiaolu, G.A.O.; Zening, X.U. Identification and classification of urban commercial districts at block scale. *Geogr. Res.* **2015**, *34*, 1125–1134.
31. Louail, T.; Lenormand, M.; Ros, O.G.C.; Picornell, M.; Herranz, R.; Frias-Martinez, E.; Ramasco, J.J.; Barthelemy, M. From mobile phone data to the spatial structure of cities. *Sci. Rep.* **2014**, *4*, 5276. [CrossRef] [PubMed]
32. Kang, C.; Gao, S.; Lin, X.; Xiao, Y.; Yuan, Y.; Liu, Y.; Ma, X. Analyzing and geo-visualizing individual human mobility patterns using mobile call records. In Proceedings of the 2010 18th International Conference on Geoinformatics, Beijing, China, 18–20 June 2010; pp. 1–7.
33. Lee, R.; Wakamiya, S.; Sumiya, K. Discovery of unusual regional social activities using geo-tagged microblogs. *World Wide Web* **2011**, *14*, 321–349. [CrossRef]
34. Yuan, J.; Zheng, Y.; Xie, X. Discovering regions of different functions in a city using human mobility and POIs. In Proceedings of the 18th ACM SIGKDD International Conference on Knowledge Discovery and Data Mining, Beijing, China, 12–16 August 2012; pp. 186–194. [CrossRef]
35. Yuan, N.J.; Zheng, Y.; Xie, X.; Wang, Y.; Zheng, K.; Xiong, H. Discovering urban functional zones using latent activity trajectories. *IEEE Trans. Knowl. Data Eng.* **2015**, *27*, 712–725. [CrossRef]
36. Long, Y.; Thill, J.C. Combining smart card data and household travel survey to analyze jobs-housing relationships in Beijing. *Comput. Environ. Urban Syst.* **2015**, *53*, 19–35. [CrossRef]

37. Liu, X.; He, J.; Yao, Y.; Zhang, J.; Liang, H.; Wang, H.; Hong, Y. Classifying urban land-use by integrating remote sensing and social media data. *Int. J. Geogr. Inf. Sci.* **2017**, *31*, 1675–1696. [CrossRef]
38. Yao, Y.; Li, X.; Liu, X.; Liu, P.; Liang, Z.; Zhang, J.; Mai, K. Sensing spatial distribution of urban land-use by integrating points-of-interest and Google Word2Vec model. *Int. J. Geogr. Inf. Sci.* **2017**, *31*, 825–848. [CrossRef]
39. Hu, T.; Yang, J.; Li, X.; Gong, P. Mapping urban land-use by using landsat images and open social data. *Remote Sens.* **2016**, *8*, 151. [CrossRef]
40. Zhang, Y.; Li, Q.; Huang, H.; Wu, W.; Du, X.; Wang, H. The combined use of remote sensing and social sensing data in fine-grained urban land use mapping: A case study in Beijing, China. *Remote Sens.* **2017**, *9*, 865. [CrossRef]
41. Li, X.; Lin, T.; Zhang, G.; Xiao, L.; Zhao, Q.; Cui, S. Dynamic analysis of urban spatial expansion and its determinants in Xiamen Island. *J. Geogr. Sci.* **2011**, *21*, 503–520. [CrossRef]
42. Shen, G.; Xu, B.; Jin, Y.; Chen, S.; Zhang, W.; Guo, J.; Liu, H.; Zhang, Y.; Yang, X. Monitoring wind farms occupying grasslands based on remote-sensing data from China's GF-2 HD satellite—A case study of Jiuquan city, Gansu province, China. *Resour. Conserv. Recycl.* **2017**, *121*, 128–136. [CrossRef]
43. Samardžić-Petrović, M.; Dragićević, S.; Kovačević, M.; Bajat, B. Modeling urban land use changes using support vector machines. *Trans. GIS* **2016**, *20*, 718–734. [CrossRef]
44. Baatz, M.; Schäpe, A. Multiresolution segmentation: an optimization approach for high quality multi-scale image segmentation. *J. Photogramm. Remote Sens.* **2000**, *58*, 12–23.
45. Yu, W.; Zhou, W.; Qian, Y.; Yan, J. A new approach for land cover classification and change analysis: Integrating backdating and an object-based method. *Remote Sens. Environ.* **2016**, *177*, 37–47. [CrossRef]
46. Zhou, W.; Troy, A. An object-oriented approach for analysing and characterizing urban landscape at the parcel level. *Int. J. Remote Sens.* **2008**, *29*, 3119–3135. [CrossRef]
47. Musa, H.D.; Yacob, M.R.; Abdullah, A.M.; Ishak, M.Y. Delphi method of developing environmental well-being indicators for the evaluation of urban sustainability in Malaysia. *Procedia Environ. Sci.* **2015**, *30*, 244–249. [CrossRef]
48. Taleai, M.; Mansourian, A. Using Delphi-AHP method to survey major factors causing urban plan implementation failure. *J. Appl. Sci.* **2008**, *8*, 2746–2751. [CrossRef]
49. Le Pira, M.; Inturri, G.; Ignaccolo, M.; Pluchino, A. Modelling consensus building in Delphi practices for participated transport planning. *Transp. Res. Procedia* **2015**, *25*, 3729–3739. [CrossRef]
50. Linstone, H.A.; Turoff, M. Delphi: A brief look backward and forward. *Technol. Forecast. Soc. Chang.* **2011**, *78*, 1712–1719. [CrossRef]
51. Baraldi, A.; Bruzzone, L.; Blonda, P. Quality assessment of classification and cluster maps without ground truth knowledge. *IEEE Trans. Geosci. Remote Sens* **2005**, *43*, 857–873. [CrossRef]
52. Whiteside, T.G.; Boggs, G.S.; Maier, S.W. Comparing object-based and pixel-based classifications for mapping savannas. *Int. J. Appl. Earth Obs. Geoinf.* **2011**, *13*, 884–893. [CrossRef]
53. Mesev, V. Fusion of point-based postal data with IKONOS imagery. *Inf. Fusion* **2007**, *8*, 157–167. [CrossRef]
54. Sohn, G.; Dowman, I. Data fusion of high-resolution satellite imagery and LiDAR data for automatic building extraction. *ISPRS J. Photogramm. Remote Sens.* **2007**, *62*, 43–63. [CrossRef]